Journal of Magnetism and Magnetic Materials 457 (2018) 126–134

Contents lists available at ScienceDirect

Journal of Magnetism and Magnetic Materials

journal homepage: www.elsevier.com/locate/jmmm

Research articles

Magnetocaloric effect, electric, and dielectric properties of $Nd_{0.6}Sr_{0.4}Mn_xCo_{1-x}O_3$ composites

I.A. Abdel-Latif [a,b,c,*], A.M. Ahmed [d], H.F. Mohamed [d], S.A. Saleh [d], J.A. Paixão [e], Kh.A. Ziq [f], M.Kh. Hamad [f], E.G. Al-Nahari [f], M. Ghozza [g], S. Allam [h]

[a] Physics Department, College of Sciences and Arts, Najran University, P.O. Box 1988, Najran 11001, Saudi Arabia
[b] Advanced Materials and Nano-Research Centre, Najran University, P.O. Box: 1988, Najran 11001, Saudi Arabia
[c] Reactor Physics Department, NRC, Atomic Energy Authority, Abou Zabaal, P.O. Box 13759, Cairo, Egypt
[d] Physics Department, Faculty of Science, Sohag University, Sohag 82524, Egypt
[e] CFisUC, Department of Physics, University of Coimbra, P-3004-516 Coimbra, Portugal
[f] Physics Department, College of Sciences, King Fahd University of Petroleum & Minerals, P.O. Box 5047, Dhahran 31261, Saudi Arabia
[g] Basic Science Department, High Institute of Engineering and Technology, El-Marg, Cairo, Egypt
[h] Physics Department, Faculty of Science, Cairo University, Giza, Egypt

ARTICLE INFO

Article history:
Received 10 November 2017
Received in revised form 17 January 2018
Accepted 27 February 2018
Available online 27 February 2018

Keywords:
Magnetic phase transition
Arrott plots
Dielectric permittivity
Magnetocaloric effect

ABSTRACT

The magnetocaloric effect (MCE) and electric-dielectric properties of the Nd-cobaltate perovskites $Nd_{0.6}Sr_{0.4}Co_{1-x}Mn_xO_3$ (x = 0, 0.3, 0.7 and 1) were investigated for possible use in magnetic cooling applications. Upon Mn substitution, the magnetic exchange interaction is affected by the (Mn^{4+}/Mn^{3+}) ratio, which in turn impacts several physical properties. The XRD patterns of the synthesized composites revealed a single phase with an orthorhombic structure with space group *Pbnm* (62). The orthorhombic lattice distortion increases linearly with the Mn content, reaching a maximum value ($D = 7.377 \times 10^{-3}$) for $Nd_{0.6}Sr_{0.4}MnO_3$. The temperature and frequency dependence of the dielectric permittivity was studied and analyzed using Maxwell-Wagner interfacial polarization and Koops phenomenological theory. The rapid increase in magnetic susceptibility around the paramagnetic (PM)–ferromagnetic (FM) transition temperature T_C is greatly affected by Mn substitution. The decrease in susceptibility with increasing temperature can be attributed to a charge ordering effect. The PM-FM transition occurs in the temperature range of 150–200 K. Moreover, the presence of spontaneous magnetization with second-order phase transitions is observed from Arrott plot isotherms. The MCE was also investigated by determining ΔS_M and the relative cooling power (RCP), and the maximum value is found for $Nd_{0.6}Sr_{0.4}Co_{0.3}$ $Mn_{0.7}O_3$. These results compare favorably with those reported for similar materials, indicating our materials as a possible candidate for use in magnetocaloric refrigerators.

1. Introduction

Progress in materials science has enabled the emergence of new materials that can be used in cooling systems, such as rare earth manganites. Magnetic refrigeration is a cooling technology that uses the magnetocaloric effect observed in these advanced materials to attain extremely low temperatures. The basic mechanism of cooling in these materials is as follows: when a magnetic material is subjected to a considerably high magnetic field, the reorientation of magnetic moments is achieved, and if this magnetic field is applied adiabatically, the temperature of the material is increased. Conversely, the temperature decreases when the magnetic field is removed. The warming and cooling process resulting from the application and removal of an external magnetic field is called the magnetocaloric effect (MCE) [1–4].

The recent advances in rare earth transition metal oxide perovskites reflect the extent of interest in basic and applied research related to these materials. Near room temperature magnetic refrigerators represent an important application in the context of environmentally friendly technology [5–10]. Moreover, their technological potential spans a wide range of applications [11–14]. Among these compounds, the manganites and cobaltates show colossal magnetoresistance [1–4,15] and MCEs [16–18]. Magnetic refrigeration uses the MCE in these materials to attain a decrease

* Corresponding author at: Physics Department, College of Sciences and Arts, Najran University, P.O. Box 1988, Najran 11001, Saudi Arabia.
E-mail address: iaalsayed@nu.edu.sa (I.A. Abdel-Latif).

https://doi.org/10.1016/j.jmmm.2018.02.087
0304-8853/

in temperature over various ranges. When the material is subjected to a sufficiently high magnetic field, a high degree of reorientation of the magnetic moments occurs. When the magnetic field is applied adiabatically, the temperature of the material is raised and, subsequently, heat is exchanged with the environment. When the magnetic field is subsequently

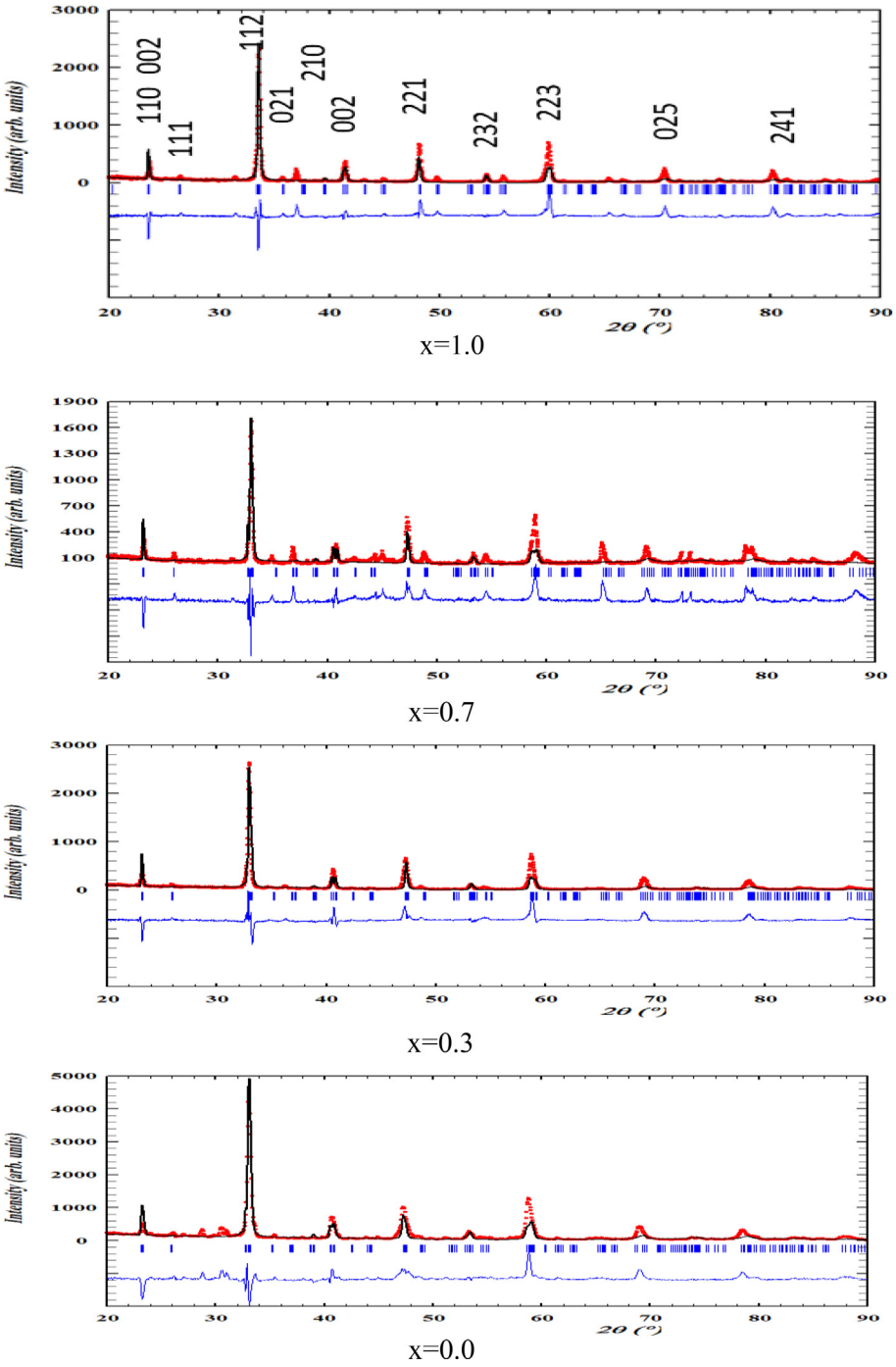

Fig. 1. XRD patterns of $Nd_{0.6}Sr_{0.4}Mn_xCo_{1-x}O_3$.

Table 1
Lattice parameters of $Nd_{0.6}Sr_{0.4}Mn_xCo_{1-x}O_3$.

X	*a* Å	*b* Å	*c* Å	V $Å^3$	D $\times10^{-3}$	M—O1	M—O2	M—O2—M	M—O1—M
0.0	5.3632(5)	5.3266(7)	7.5499(10	215.68(5)	1.04	1.9374(2)	1.72029(12)	149.615(19)	153.94(3)
0.3	5.4524(5)	5.4094(6)	7.6682(6)	226.17(4)	2.98	1.9678(15)	1.74824(12)	149.624(17)	153.925(2)
0.7	5.4605(4)	5.4035(4)	7.6944(6)	227.03(3)	3.839	1.9743(15)	1.74966(9)	149.567(12)	153.972(2)
1.0	5.4646(7)	5.4107(10)	7.6519(13)	226.74(6)	7.377	1.9598(3)	1.75411(15)	149.78(2)	153.70(4)

removed, a further decrease in the temperature is observed [19–22].

Magnetic entropy is commonly determined by evaluating the magnetic entropy ΔS_M (T, H) using isothermal magnetization measurements. In an isothermal process of magnetization, the total magnetic entropy change of the system due to the application of a magnetic field, ΔS_M, can be determined from Maxwell's relation $(dS/dH)_T = (dM/dT)_H$ using [19]:

$$\Delta S_M = S_M(T,H) - S_M(T,0) = \int_0^H (dM(T,H)/dT)_H dH \quad (1)$$

Numerical integration of two consecutive isothermal M(H) curves around the mean temperature $T = 1/2(T_{i+1} + T_i)$ allows us to approximately determine ΔS_M (T, H) [14] by

$$\Delta S_M(T,H) = \sum_i \frac{1}{(T_{i+1} + T_i)} [M_{i+1}(T_{i+1},H) - M_i(T_i,H)]\Delta H \quad (2)$$

The relative cooling power (RCP), which is often used to indicate the potential of magnetocaloric materials, is given as[20]:

$$RCP = |\Delta S|^{max} \delta T_{FWHM} \quad (3)$$

where $|\Delta S|^{max}$ is the maximum value of the change in magnetic entropy and δT_{FWHM} is the full width at half maximum (FWHM) of the peak in the entropy change.

The dielectric permittivity of solids is a measure of the extent to which the electric charge distribution in the material can be distorted or polarized by applying an electric field [23,24]. Understanding the behavior of dielectrics with variations in the field, temperature and frequency is of particular importance in current electronic applications.

In the present paper, the electric, dielectric, and magnetic properties and MCE of $Nd_{0.6}Sr_{0.4}Co_{1-x}Mn_xO_3$ have been investigated. Our results showed that the highest value of ΔSM near T_c in $Nd_{0.6}Sr_{0.4}Mn_xCo_{1-x}O_3$ (x = 0, 0.3, 0.7 and 1) was for x = 0.7, enabling us to conclude that this compound is promising for magnetic cooling applications.

2. Experimental details

Nanocomposites $Nd_{0.6}Sr_{0.4}Co_{1-x}Mn_xO_3$ (x = 0, 0.3, 0.7 and 1) were prepared using the co-precipitation method by dissolving high purity chlorides of neodymium, strontium, cobalt and manganese in 100 ml and adding to the solution pure sodium hydroxide with the proper molar ratio until pH 12–13 was reached. Precipitated $Nd_{0.6}Sr_{0.4}Mn_xCo_{1-x}O_3$ was washed with distilled water to remove all formed NaCl [25]. The dried precipitate was fired at 850 °C for 12 h. XRD measurements were performed with Cu radiation using a PANalytical X'pert Pro MPR diffractometer. A JEOL field emission-scanning electron microscope (FE-SEM, JSM-5600) with an acceleration voltage of 15 kV and a magnification of ×43000 was used to obtain micrographs and to conduct elemental analysis measurements. The magnetization isotherms of $Nd_{0.6}Sr_{0.4}Mn_xCo_{1-x}O_3$ were measured using a Dynacool Quantum Design physical properties measuring system (PPMS) in a range of temperature from 2 K to 300 K.

3. Results and discussions

3.1. Crystal structure

All the measured X-ray diffraction patterns of $Nd_{0.6}Sr_{0.4}Mn_xCo_{1-x}O_3$ were analyzed using Fullprof software [26]. The X-ray diffraction patterns are shown in Fig. 1. All the reflections belong to the orthorhombic crystal system of the *Pbnm* space group (No. 62) with maximum reflection intensity in the (1 1 2) plane. No impurity phases were detected. The refined lattice parameters are listed in table 1, and the crystal structure of $Nd_{0.6}Sr_{0.4}Mn_{0.3}Co_{0.7}O_3$ is represented in scheme 1. The Nd/Sr atoms

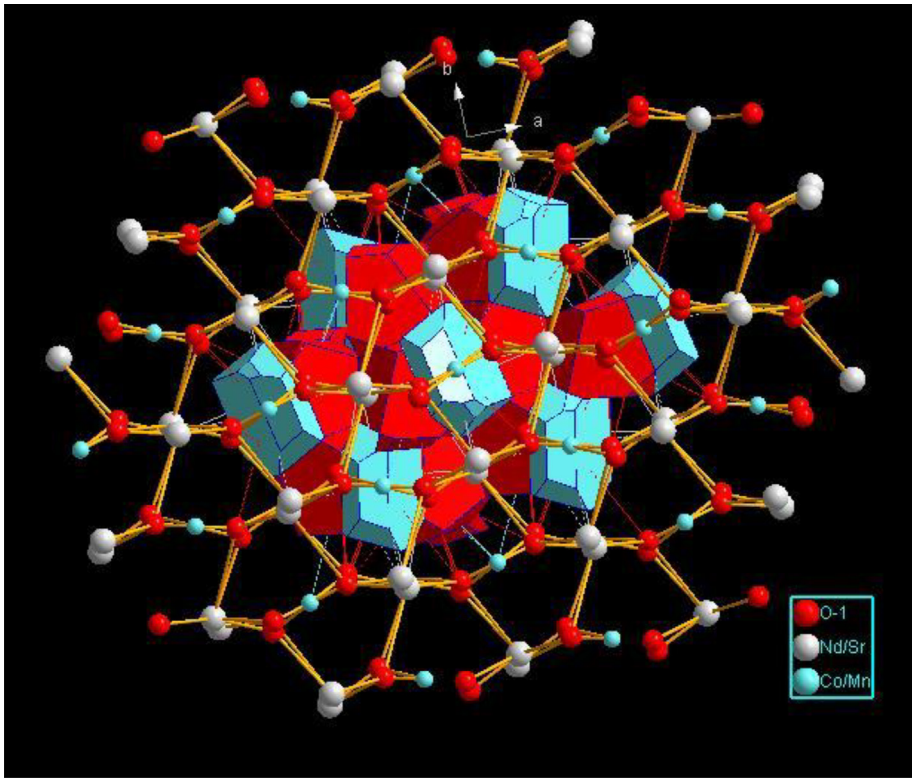

Scheme 1. The crystal structure representation of $Nd_{0.6}Sr_{0.4}Mn_{0.3}Co_{0.7}O_3$.

occupy the (x, 1/4, z) position. The Mn/Co atoms occupy the (0, 0, 1/2) position and are surrounded by octahedral oxygen atoms. The oxygen atoms in this compound are distributed as follows: four of them occupy the (x, 1/4, z) position, and eight of them occupy the (x, y, z) position. The bond lengths between Mn/Co— O and the Mn/Co—O—Mn/Co bond angles were calculated and are listed in table 1. The Mn/Co—O_1 bond length is observed to increase with increasing manganese concentration, i.e., for x = 0, 0.3 and 0.7; however, it decreased for x = 1. This differences in the bond length resulted from the oxygen atoms occupying different positions and the tilt in the octahedral sites.

Table 2
Crystalline size and phase transition temperature of $Nd_{0.6}Sr_{0.4}Mn_xCo_{1-x}O_3$.

X	*Grain Size* *nm*	T_c *K*	E_A eV	Possible Magnetic state
0.0	74.8	10	0.142	FM below 10 K
0.3	113.5	165	0.609 0.160	AF below 165
0.7	147.4	130	0.133	AF below 150
1.0	34.2	45	0.215	FM below 45

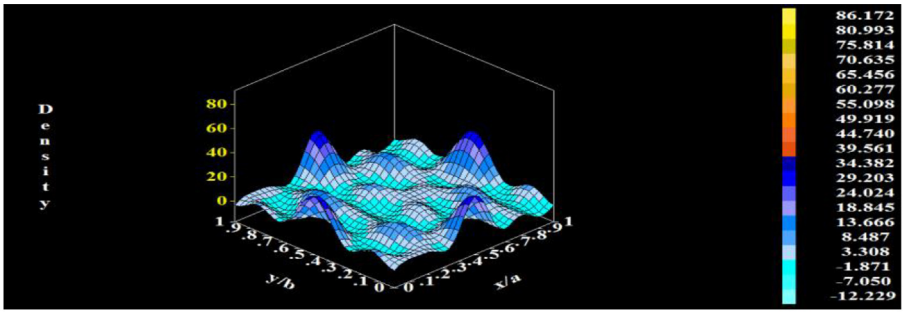

x=0

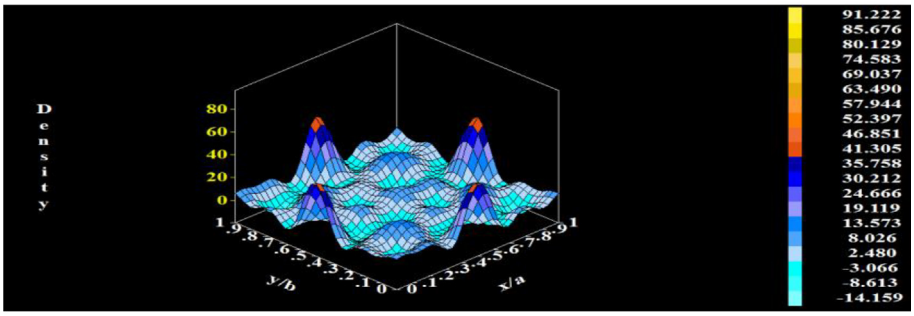

x=0.3

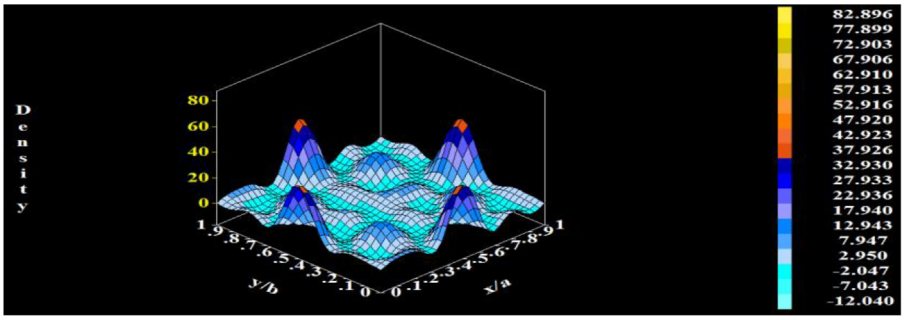

x=0.7

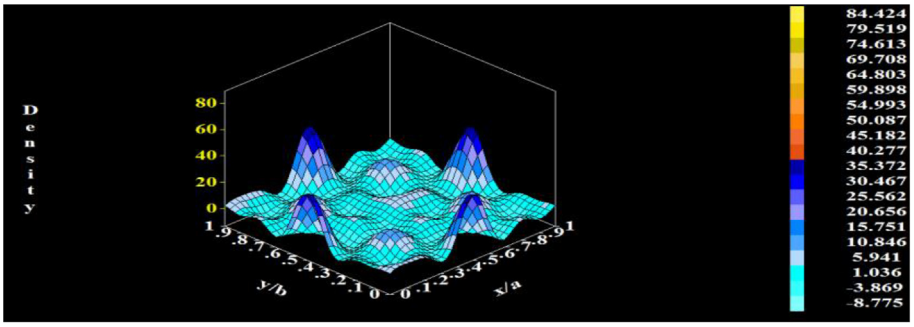

x=1

Fig. 2. Electron density of $Nd_{0.6}Sr_{0.4}Mn_xCo_{1-x}O_3$.

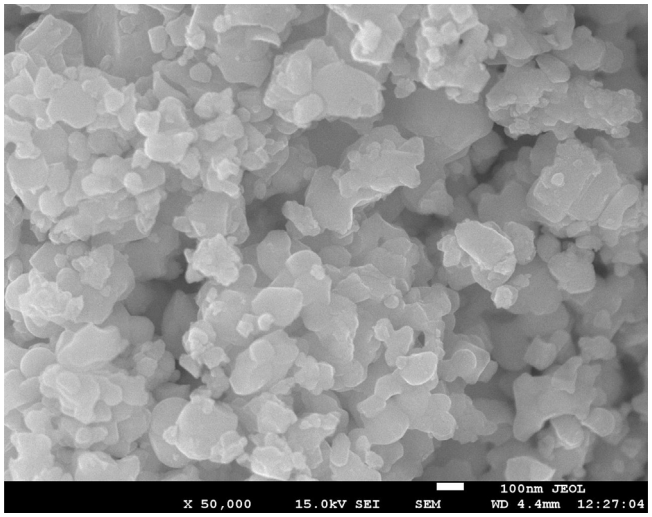

Fig. 3. Micrograph of $Nd_{0.6}Sr_{0.4}Mn_{0.7}Co_{0.3}O_3$.

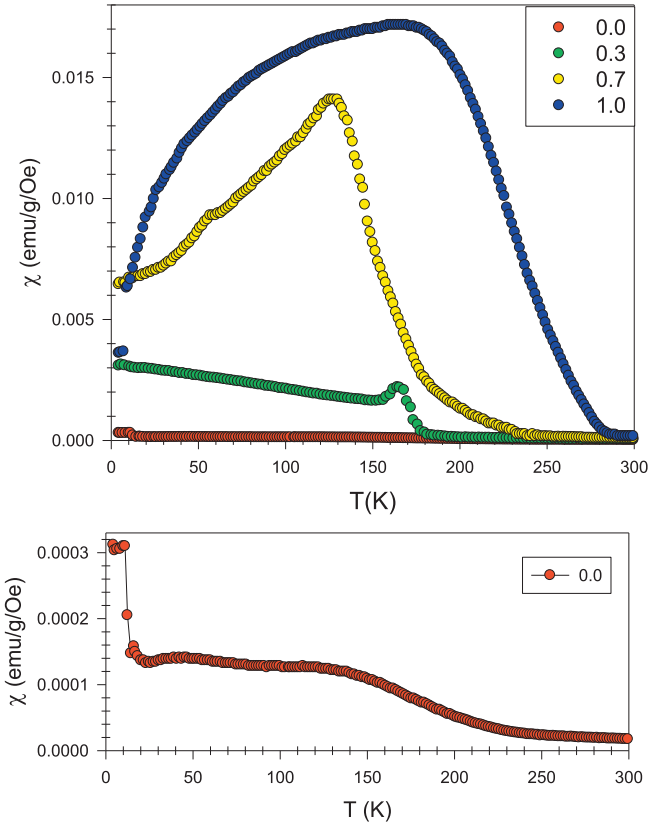

Fig. 4. The variations of the susceptibility with temperature.

Distortion of the ideal perovskite structure is very important parameter because it correlates with electrical and magnetic properties. The obtained distortion, D, was calculated according to the following relation [27]:

$$D = \frac{1}{3}\sum_{i=1}^{3}\left|\frac{a_i - \bar{a}}{a_1}\right|, \quad \text{where } a_1 = a,\ a_2 = b,\ a_3 = \frac{c}{\sqrt{2}} \quad \text{and}$$

$$\bar{a} = \left[\frac{a.b.c}{\sqrt{2}}\right]^{\frac{1}{3}}$$

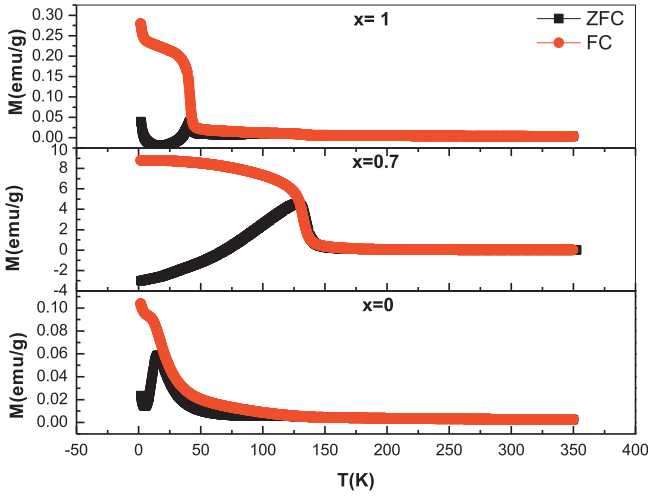

Fig. 5. Magnetization vs. temperature curves of $Nd_{0.6}Sr_{0.4}Mn_xCo_{1-x}O_3$ (x = 0, 0.7 and 1 at.%) measured under ZFC and FC condition in a magnetic field of 100 Oe of $Nd_{0.6}Sr_{0.4}Mn_{0.7}Co_{0.3}O_3$ (x = 0, 0.7 and 1).

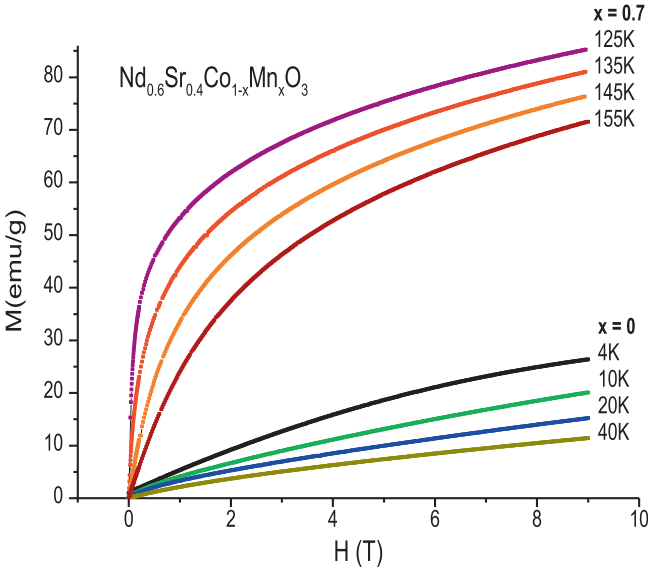

Fig. 6. Magnetic moment dependence on magnetic field at different temperatures of $Nd_{0.6}Sr_{0.4}Mn_{0.7}Co_{0.3}O_3$ (x = 0 and 0.7).

The numerical values of the distortion D of the perovskite structure are given in Table 1. The value of D is smallest (1.044×10^{-3}) for the pure cobalt perovskite $Nd_{0.6}Sr_{0.4}CoO_3$ and then increases almost linearly with the manganese content, reaching its maximum value (7.377×10^{-3}) for the pure manganite $Nd_{0.6}Sr_{0.4}MnO_3$. The structural stability of perovskites depends on the size of their constituent atoms, which determines the distortion factor D.

The electron density inside a $Nd_{0.6}Sr_{0.4}Mn_xCo_{1-x}O_3$ unit cell is calculated using the **F**ast **F**ourier **T**ransform (**FFT**), a subprogram available in Fullprof. The electron density is calculated according to the following expression [28]:

$$\rho(r) = \frac{1}{V}\sum_{H} F(H)e^{-2\pi i(H.r)}$$

where ***V*** is the volume of the $Nd_{0.6}Sr_{0.4}Co_{1-x}Mn_xO_3$ unit cell, ***H*** is the reciprocal lattice vector, ***r*** is the vector position inside the unit

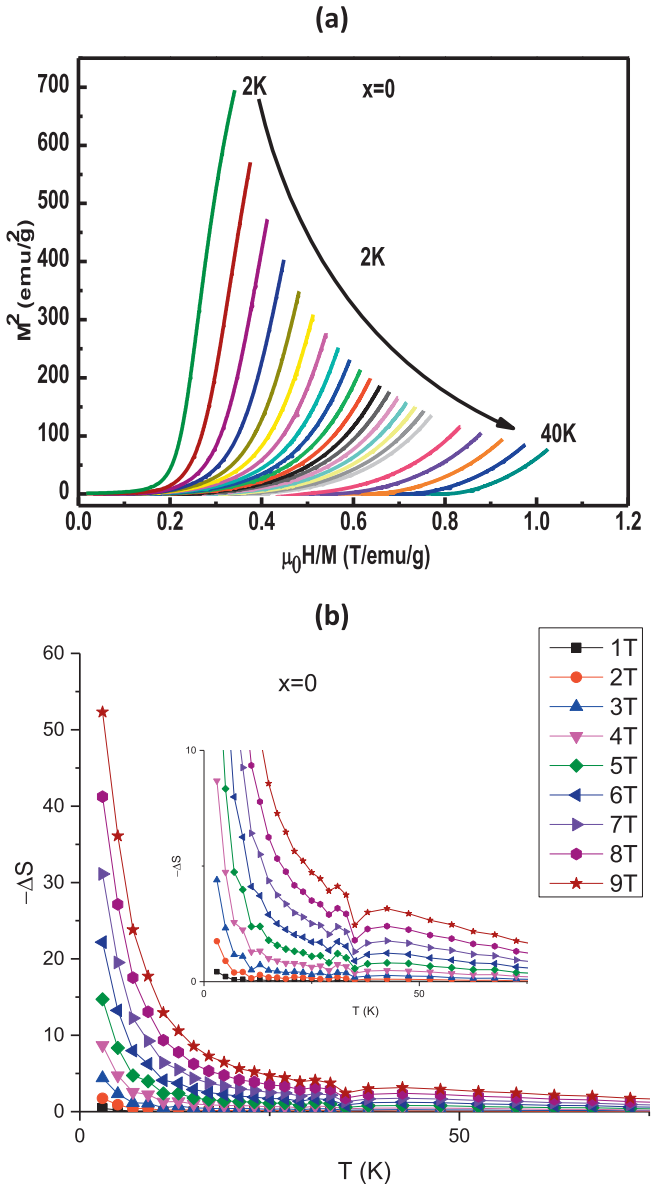

Fig. 7. Magnetic properties of $Nd_{0.6}Sr_{0.4}Mn_{0.7}Co_{0.3}O_3$ (x = 0); (a) Arrott plots around T_C measured at selected temperatures (b) magnetic entropy as a function of temperatures.

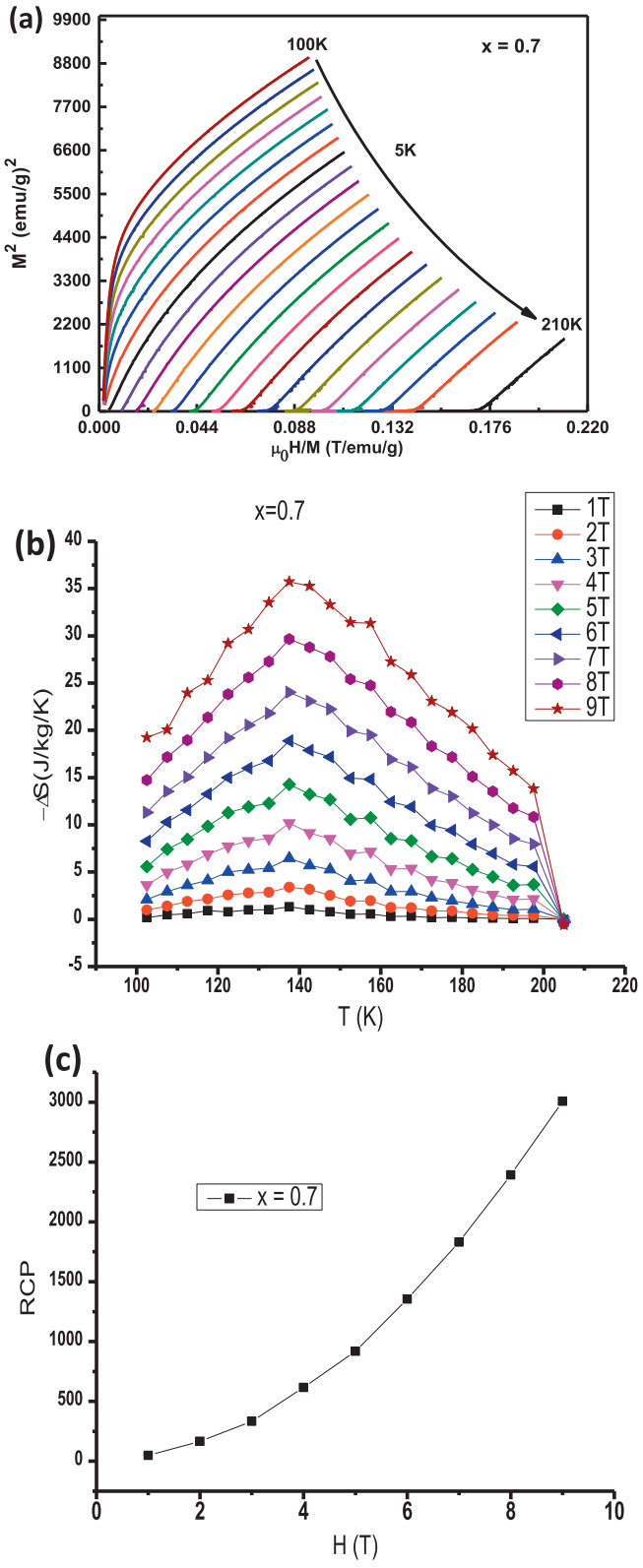

Fig. 8. Magnetic properties of $Nd_{0.6}Sr_{0.4}Mn_{0.7}Co_{0.3}O_3$ (x = 0); (a) Arrott plots around T_C measured at selected temperatures (b) magnetic entropy as a function of temperatures (c) RCP as a function magnetic field.

cell, and $F(\boldsymbol{H})$ are complex Fourier coefficients used to perform different types of Fourier syntheses. The units of $\rho(\boldsymbol{r})$ are those of $F(\boldsymbol{H})$ divided by those of V. The resulting electron density maps inside the unit cell of $Nd_{0.6}Sr_{0.4}Co_{1-x}Mn_xO_3$ are calculated and are shown in Fig. 2. Clearly, the density of electrons along the c-axis for $Nd_{0.6}Sr_{0.4}Co_1O_3$ (x = 0.0) is lower than that for samples with higher manganese concentrations. The electron density ultimately affects the electrical conductance and magnetic ordering in these perovskite materials.

The crystalline size (δ) are calculated using the well-known Scherrer formula; [29]

$$\delta = k\lambda/(B\sin\theta)$$

where B is the FWHM and is equal to $B_{obs.} - B_{std.}$ ($B_{obs.}$ is the FWHM of an observed sample, and $B_{std.}$ is the FWHM of a standard sample). The crystalline size of $Nd_{0.6}Sr_{0.4}Mn_xCo_{1-x}O_3$ is listed in Table 2. The particle size is smallest (δ = 34 nm) for x = 1, then increases to a maximum particle size of approximately 147 nm for x = 0.7, and finally decreases to 75 nm for x = 0.

The SEM microstructure graphs of $Nd_{0.6}Sr_{0.4}Co_{0.3}Mn_{0.7}O_3$ are shown in Fig. 3. There is clearly homogeneity in the crystalline size

throughout the graph. The mean value of the particle size of $Nd_{0.6}Sr_{0.4}Mn_{0.7}Co_{0.3}O_3$ is 150.80 nm, as determined from the SEM graphs, which agrees with the crystalline size deduced from the XRD measurements (147 nm).

3.2. Susceptibility measurements

The variations in the magnetization M under field cooled (FC) and zero field cooled (ZFC) conditions with temperature in H = 100 Oe are presented in Fig. 4. The FC protocol revealed that all samples undergo a ferromagnetic (FM)-paramagnetic (PM) phase transition at a certain temperature (T_c). The ZFC curves showed a peak near the Curie temperature T_c. Both the FC and ZFC curves become reversible at temperatures higher than the T_c, as shown in Fig. 5. The sample with x = 0.0 showed week susceptibility and a low temperature plateau that extends up to 10.5 K. The irreversible behavior is similar to cluster-glass behavior, as previously reported for other manganite [30] and cobaltate [31,32] systems. The possible magnetic states, along with the T_C and Co content, are given in Table 2.

3.3. Magnetization and magnetocaloric effect (MCE)

To evaluate the MCE, the isothermal magnetization (Fig. 6) was measured at different temperatures in a magnetic field up to 9 Tesla. The M(H) of the sample with x = 0 increases rapidly at H < 3 T and slowly above 3 T without reaching the saturation state. The Arrott plots are shown in Fig. 7 and Fig. 8. By contrast, the M (H) isotherms of the sample with x = 0.7 increase rapidly at H < 1 T, reaching saturation just above 2 T. This result confirms the FM behavior for the sample with x = 0.7. Fig. 7 illustrates the Arrott plots (M^2 versus $\mu_0 H/M$) determined from the magnetization isotherms for the x = 0, 0.7 and 1 samples. The curves clearly exhibit a positive slope throughout the entire M^2 range, which confirms the occurrence of a second-order phase transition according to the Banerjee criterion: a transition is second order if all the Arrott plots have a positive slope [33,34]. Fig. 7 and Fig. 8 illustrate the temperature dependence of the magnetic entropy change ΔS_M (T, H) for $Nd_{0.6}Sr_{0.4}Mn_xCo_{1-x}O_3$ nanocomposites experiencing different strength magnetic fields. As shown in Fig. 8, the negative ΔS_M exhibits a peak around the Curie temperature T_C for the x = 0.7 sample, whereas the other samples exhibit a small peak near T_{irr} (which appears above the T_C). The peak magnitude and position increase as the magnetic field strength increases. The highest value of $\Delta S_M^{(max)}$ in our case was 6.46 J/kg K for $Nd_{0.6}Sr_{0.4}Co_{0.3}Mn_{0.7}O_3$. Moreover, the peak of $\Delta S_M^{(max)}$ is very broad because of a second-order phase transition. For $Nd_{0.6}Sr_{0.4}Co_{0.3}Mn_{0.7}O_3$, the RCP is evaluated using different applied magnetic fields, and the results are plotted in Fig. 8. The figure reveals that the observed RCP nonlinearly increases with the applied field, reaching 333.16 J kg^{-1} at 3 T. This value then increased to 917.13 Jkg^{-1} at 5 T and 3007.14 Jkg^{-1} at 9 T. A comparison between the ΔS_M and RCP of $Nd_{0.6}Sr_{0.4}Co_{0.3}Mn_{0.7}O_3$ and those for other materials [22,38–44] is shown in table 3. The obtained values for our sample are comparable to those obtained for the traditional and more expensive pure Gd element, suggesting the possibility of using $Nd_{0.6}Sr_{0.4}Co_{0.3}Mn_{0.7}O_3$ in magnetic refrigerators. In perovskite manganites, the mechanisms that govern the magnetic property of the materials are the antiferromagnetic superexchange interaction in the $Mn^{3+}(Co^{3+})—O^{2-}—Mn^{3+}(Co^{3+})/Mn^{4+}(Co^{4+})—O^{2-}—Mn^{4+}(Co^{4+})$ bonds and the FM double-exchange interaction in the $Mn^{3+}(Co^{3+})—O^{2-}—Mn^{4+}(Co^{4+})$ bonds [35,36]. The relative strength of these two interactions can be powerfully influenced by the oxygen efficiency [37]. The cation distributions in the B-site plays very important role in the electrical and the magnetic transport in perovskites.[45–47] According to Bashkirov el al., [46,47] the $NdFe_xMn_{1-x}O_3$ and $SmFe_xMn_{1-x}O_3$ orthoferrites showed several nonequivalent sites of the iron ions where different sextets were observed corresponding to different number of the Fe ions in the next nearest neighboring. They suggested a nonrandom cation distribution model in such compounds to interpret the multi-sextets spectra [47]. Similarly, in our case cobalt and manganese may occupy several nonequivalent sites and this may lead to the different types of the magnetic exchange between manganese and cobalt; $Co^{+3}—Co^{+3}$, $Co^{+3}—Co^{+4}$, $Co^{3+}—Mn^{+3}$, $Co^{3+}—Mn^{+4}$, $Co^{4+}—Mn^{+3,}$ $Mn^{+3}—Mn^{+3}$, and $Mn^{+3}—Mn^{+4}$.

Table 3
Typical magnetic parameters used for magnetic refrigeration.

Sample	T_c (K)	$-\Delta S_{max}$ (J Kg^{-1} K^{-1})	RCP (J/kg)	ΔH (T)	Reference of data
$Nd_{0.6}Sr_{0.4}Mn_{0.7}Co_{0.3}O_3$	150	6.46	333.16	3	Present
		14.27	917.75	5	work
		35.73	3007.14	9	
$La_{0.65}Ca_{0.35}Mn_{0.9}Ti_{0.1}O_3$	103	1.3		3	Ref. [20]
$La_{0.8}Ba_{0.1}Ca_{0.1}Mn_{0.85}Co_{0.15}O_3$	205	1.63	57.52	3	Ref. [38]
$La_{0.67}Sr_{0.33}Mn_{0.9}Cr_{0.1}$ O_3	328	5.0		5	Ref. [22]
DyNiSi	8.8	5.9	99	5	Ref. [39]
$Mn_{0.89}Fe_{0.11}NiGe$	203	−25.8		3	Ref. [40]
$TmFeO_3$	17	12	260	7	Ref. [41]
$Pr_{0.6}Pb_{0.}4MnO_3$	240	3.9		1.4	Ref. [42]
NiFeCoCrPd0.5		3	36	1	Ref. [43]
$Pr_{1.75}Sr_{1.25}Mn_2O_7$	305	3.06	339	7	Ref. [44]

3.4. Dielectric and electric measurements

The dielectric permittivity (ε*) of a material is represented as $\varepsilon^* = \varepsilon_r \varepsilon_0$, [23] where ε_r, the relative permittivity of that material, is related to a variety of physical phenomena that contribute to the polarization of the dielectric material and ε_0 is free space permittivity. The various assumptions made in our discussion can be better appreciated by studying the variations in ε* with frequency and temperature. The variation in permittivity as a function of frequency for $Nd_{0.6}Sr_{0.4}Mn_xCo_{1-x}O_3$ (x = 0, 0.3 and 0.7) fired at 850° C is plotted at different temperatures, as shown in Fig. 9. The same behavior is observed for all samples: the dielectric permittivity decreases with increasing frequency. In the low frequency region, very high dielectric permittivity was observed, whereas in the high frequency region, the dielectric permittivity decreases to a very small value and becomes approximately independent of the frequency. The observed dielectric behavior can be explained in term of Maxwell-Wagner interfacial polarization and Koops phenomenological theory [24]. According to this model, space-charge polarization arises because of the inhomogeneous dielectric structure of the material. The structure comprises large well-conducting grains separated by poorly conducting (or resistive) grain boundaries. The grain boundaries are found to be more effective at lower frequencies, whereas the grains are effective at higher frequencies. The grain boundaries are formed during the sintering process because of the superficial reduction or oxidation of crystallites [48]. The frequency-independent behavior of all samples at higher frequency is simply due to the charge carriers, which are responsible for different mechanisms of polarization. Usually, the dipolar, electronic, ionic, and interfacial polarizations contribute to the dielectric constant of any material. At low frequencies, the dipolar and interfacial polarizations are effective to the dielectric constant. By contrast, at higher frequencies, the electronic polarization is effective, and the dipolar contribution becomes insignificant. In other words, the higher value of the dielectric permittivity at lower frequencies may be attributed to the presence of a different type of polarization in a particular space-charge polarization. Conversely, a nearly constant value of dielectric permittivity was observed at higher frequency because of the absence of space-charge polariza-

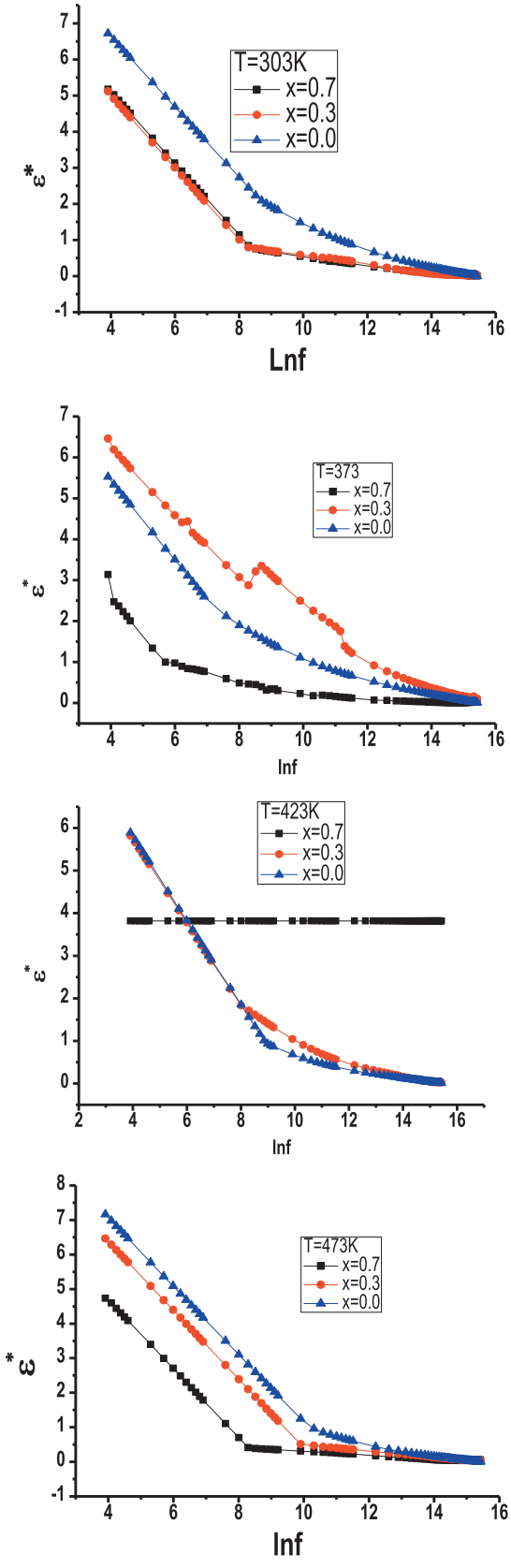

Fig. 9. The dependence of permittivity on frequency in $Nd_{0.6}Sr_{0.4}Mn_xCo_{1-x}O_3$ (x = 0, 0.3 and 0.7) at different temperatures.

tion [49]. Moreover, the dielectric materials polarize via one of the three mechanisms, i.e., electronic, ionic or orientation polarization

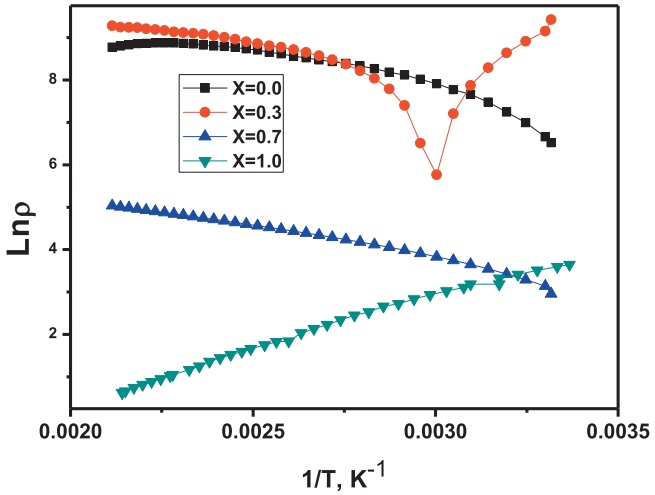

Fig. 10. The dependence of DC resistivity on temperature in $Nd_{0.6}Sr_{0.4}Mn_xCo_{1-x}O_3$.

[50]. The electronic polarization and conduction mechanisms are similar [51].

The electrical properties of any material is an important factor in helping us understand the nature of that material and in providing us with reliable information about its transport phenomenon and other physical properties. To determine the general behavior of electrical resistivity and obtain information about current transport mechanisms, the variation in the DC resistivity of $Nd_{0.6}Sr_{0.4}Mn_xCo_{1-x}O_3$with temperature was measured and analyzed (see Fig. 10) to distinguish between the possible mechanisms in the tested samples, namely, band transfer, thermionic emission, thermally assisted tunneling and variable-range hopping. There is a clear decrease in resistivity with increasing temperature, which explains the semiconducting behavior of all these compounds except $Nd_{0.6}Sr_{0.4}Mn_{0.3}Co_{0.7}O_3$, which exhibits a transition point near 333 K. The electrical resistivity could be written as a function of temperature using the Arrhenius equation [52]:

$$\rho = \rho_o \exp(E_{th}/K_B T)$$

where ρ_o is a preexponential coefficient, E_{th} is the thermal activation energy, K_B is Boltzmann's constant and T is the absolute temperature. According to the linear dependence, the thermal activation energy can be calculated, which has a value of ~0.215 eV for $Nd_{0.6}Sr_{0.4}MnO_3$ with a positive slope. The activation energy is ~0.133 eV and 0.142 eV for $Nd_{0.6}Sr_{0.4}CoO_3$ and $Nd_{0.6}Sr_{0.4}Mn_{0.3}Co_{0.7}O_3$, respectively, with a negative slope. In the $Nd_{0.6}Sr_{0.4}Mn_{0.7}Co_{0.3}O_3$ sample, we observed a linear dependence of lnρ on temperature but with both negative and positive slopes, leading to calculated activation energies of 0.160 eV and 0.609 eV respectively. Sh. Khan et al. observed similar behavior for CuO [53], where the difference in activation energy for the same structure was attributed to the CuO morphology. Electron transport in a semiconductor material depends on the number of carriers and on the mobility of these carriers [54]. Therefore, those two factors are very important in understanding the conductivity (or resistivity) behavior in our case. If there is a change in the mobility or the number of the carriers, it may lead to a change in the conductivity or resistivity. Therefore, in our system, the change in the activation energy sign with temperature can be attributed to the change in the number of negative electrons compared to the number of positive holes.

4. Conclusions

Based on the temperature and frequency dependence of the dielectric permittivity, grain boundaries are found to be more

effective at lower frequencies, whereas the bulk grains are effective at higher frequencies. The decrease in susceptibility with increasing temperature can be attributed to a charge ordering effect. The PM-FM transition occurs in the temperature range of 150–200 K, and second-order phase transitions are observed in our samples. The maximum MCE was found for $Nd_{0.6}Sr_{0.4}Co_{0.3}Mn_{0.7}O_3$, and it compares favorably with those reported for other materials, allowing us to conclude that it is a promising candidate for use in magnetocaloric refrigerators. The several nonequivalent sites of the cobalt–manganese ions corresponding to different number of the Co and/or Mn ions in the next nearest neighboring may play very important in both electric and magnetic transport.

Acknowledgment

The author is thankful to the Deanship of Scientific Research for Grant Research code NU/ESCI/14/019 to Dr. I. A. Abdel-Latif, Najran University, Saudi Arabia. This work was partially supported by funds from FEDER (Programa Operacional Factores de Competitividade COMPETE) and from FCT-Fundação para a Ciência e a Tecnologia under the Project No. UID/FIS/04564/2016. Access to TAIL-UC facility funded under QREN-Mais Centro Project No. ICT_2009_02_012_1890 and is gratefully acknowledged. Work done at King Fahd University of Petroleum and Minerals was supported by project IN121002.

References

[1] M.S. Anwar, F. Ahmed, S.R. Lee, R. Danish, B.H. Koo, Jpn. J. Appl. Phys. 52 (2013), 10MC12.
[2] A. Selmi, R. M'nassri, W. Cheikhrouhou-Koubaa, N. Chniba Boudjada, A. Cheikhrouhou, J. Alloys Compd. 619 (2014) 626.
[3] I. Hussain, M.S. Anwar, J.W. Kim, K.C. Chung, B.H. Koo, Ceram. Int. l42 (2016) 13098–13103.
[4] A.G. Gamzatov, A.M. Aliev, A.R. Kaul, J. Alloys Compd. 710 (2017) 292–296.
[5] O. Tegus, E. Brück, K.H.J. Buschow, F.R. de Boer, Nature 415 (2002) 150–152.
[6] T. Krenke et al., Nat. Mater. 4 (2005) 450–454.
[7] Y. Fang et al., Sci. Rep. 6 (2016) 33448, https://doi.org/10.1038/srep33448.
[8] Y. Li et al., Mater. Des. 114 (2017) 410–415.
[9] W. Eerenstein, M. Wiora, J.L. Prieto, J.F. Scott, N.D. Mathur, Nat. Mater. 6 (2007) 348–351.
[10] Jian Liu, Tino Gottschall, Konstantin P. Skokov, James D. Moore, Oliver Gutfleisch, Nature Materials 11 (2012) 620–626, https://doi.org/10.1038/nmat3334.
[11] A. Dhahri et al., J. Alloys. Comp. 618 (2015) 488–496.
[12] S. Jin, T.H. Tiefel, M. Mc Cormak, R.A. Fastnacht, R. Ramesh, L.H. Chen, Science 264 (1994) 413.
[13] I.A. Abdel-Latif et al., J. Alloys. Comp. 452 (2008) 245.
[14] A. Moreo, S. Yunoki, E. Dagotto, Science 283 (1999) 2034.
[15] B. Liu et al., Mater. Des. 89 (2016) 715–720.
[16] M. Khlifi, M. Bejar, O.E.L. Sadek, E. Dhahria, M.A. Ahmed, E.K. Hlil, J. Alloys. Compds. 509 (2011) 7410–7415.
[17] S. Ghodhbane, A. Dhahri, N. Dhahri, E.K. Hlil, J. Dhahri, J. Alloys. Compds. 550 (2013) 358–364.
[18] A.M. Ahmed et al., Solid State Sci. 57 (2016) 1–8.
[19] Z.B. Guo, Y.W. Du, J.S. Zhu, H. Huang, W.P. Ding, D. Feng, Phys. Rev. Lett. 78 (1997) 1142.
[20] X. Bohigas, J. Tejada, E. Del Barco, X.X. Zhang, M. Sales, Appl. Phys. Lett. 73 (1998) 390.
[21] A.N. Vasiliev et al., J. Phys. Soc. Jpn. 82 (2013) 044714.
[22] Young Sun, Wei Tong, Yuheng Zhang, JMMM 232 (2001) 205.
[23] S.O. Nelson, J. Microwave Power Electromagn. Energy 44 (2) (2010) 98–113.
[24] M.M. Hassan, A.S. Ahmed, M. Chaman, A.H. Wasi Khan, Ameer Azam Naqvi, Mater. Res. Bull. 47 (2012) 3952–3958.
[25] I.A. Abdel-Latif, A. Al-Hajary, H. Hashem, M.H. Ghoza, Th. El-Sherbini, AIP Conf. Proc. 1370 (2011) 158–164.
[26] J. Rodriguez-Carvajal, Phys. B 192 (1993) 55.
[27] I.A. Abdel-latif, IOP Conf. Series: Mater. Sci. Eng. 146 (2016) 012003, https://doi.org/10.1088/1757-899X/146/1/012003.
[28] I.A. Abdel-Latif, M.R. Ahmed, I.A. Al-Omari, A. Sellai, JMMM 420 (2016) 363–370.
[29] A. Maihnan, C. Martin, F. Damay, B. Raveau, J. Hei-jtmanek, Phys. Rev. B. 54 (1996) 9267.
[30] D.H.N. Nam, K. Jonason, P. Nordblad, N.V. Khiem, N.X. Phuc, Phys. Rev. B. 59 (1999) 4189.
[31] A.M. Ahmed, G. Papavassiliou, H.F. Mohamed, E.M.M. Ibrahim, JMMM 392 (2015) 27.
[32] N.S. Bingham, M.H. Phan, H. Srikanth, M.A. Torija, C. Leighton, J. Appl. Phys. 106 (2009) 02390.
[33] M.H. Phan, S.C. Yu, N.H. Hur, Y.H. Yeong, J. Appl. Phys. 96 (2004) 1154.
[34] R. Mnassri, W. Cheikhrouhou-Koubaa, M. Koubaa, N. Boudjada, A. Cheikhrouhou, Solid State Commun. 151 (2011) 1579.
[35] W.J. Hu, J. Du, B. Li, Q. Zhang, Z.D. Zhang, Appl. Phys. Lett. 92 (2008) 192505.
[36] N.K. Singh, K.G. Suresh, A.K. Nigam, Solid State Commun. 127 (2003) 373–377.
[37] B.C. Tofield, W.R. Scott, J. Solid State Chem. 100 (1974) 183.
[38] M.A. Gdaiem et al., Mater. Res. Bull. 88 (2017) 91–97.
[39] H. Zhang et al., Sci. Rep. 5 (2015) 11929, https://doi.org/10.1038/srep11929.
[40] K. Xu et al., Sci. Rep. 7 (2017) 41675, https://doi.org/10.1038/srep41675.
[41] Y.-J. Ke et al., Sci. Rep. 6 (2016) 19775, https://doi.org/10.1038/srep19775.
[42] M.-H. Phan et al., J. Appl. Phys. 99 (2006) 08Q108.
[43] D.D. Belyea et al., Sci. Rep. 5 (2015) 15755, https://doi.org/10.1038/srep15755.
[44] A.O. Ayaş, M. Akyol, S.K. Çetin, M. Kaya, İ. Dinçer, An Ekicibil, Y. Elerman,, Philos. Mag. (2017), https://doi.org/10.1080/14786435.2017.1279363.
[45] V.V. Parfenov et al., Russ. Phys. J. 46 (10) (2003) 979.
[46] Sh. Bashkirov et al., Bull. Russ. Acad. Sci. 67 (7) (2003) 1165–1169.
[47] Sh.Sh. Bashkirov et al., J. Alloys Compd. 387 (2005) 70–73.
[48] M.A. El Hiti, JMMM 192 (1999) 305–313;
P.V. Reddy, T.S. Rao, J. Less Common Met. 86 (1982) 255–261.
[49] S. Mohanty, R.N.P. Choudhary, R. Padhee, B.N. Parida, Ceram. Int. 40 (2014) 9017–9025.
[50] A. Mahmoud, M.F. Warsi, M.N. Ashiq, M. Sher, Mater. Res. Bull. 47 (2012) 4197–4202.
[51] M.J. Iqbal, M.N. Ashiq, I.H. Gul, JMMM 322 (2010) 1720–1726.
[52] A.P. Moura, L.S. Cavalcante, J.C. Sczancoski, D.G. Stroppa, E.C. Paris, A.J. Ramirez, J.A. Varela, E. Longo, Adv. Powder Technol. 21 (2010) 197–202.
[53] Sher Bahadar Khan et al., New J. Chem. 37 (2013) 1098–1104.
[54] V. Kazukauskas et al., Opt. Mater. 32 (2010) 1676–1680.